

MORPHOLOGIES AND SPECTRAL ENERGY DISTRIBUTIONS OF EXTREMELY RED GALAXIES IN THE GOODS-SOUTH FIELD^{1,2}

LEONIDAS A. MOUSTAKAS³, STEFANO CASERTANO³, CHRIS CONSELICE⁴, MARK E. DICKINSON³, PETER EISENHARDT⁵, HENRY C. FERGUSON³, MAURO GIAVALISCO³, NORMAN A. GROGIN⁶, ANTON M. KOEKEMOER³, RAY A. LUCAS³, BAHRAM MOBASHER³, CASEY PAPOVICH⁷, ALVIO RENZINI⁸, RACHEL S. SOMERVILLE³, DANIEL STERN⁵

Submitted to the Astrophysical Journal Letters

ABSTRACT

Using U' - through K_s -band imaging data in the GOODS-South field, we construct a large, complete sample of 275 “extremely red objects” (EROs; $K_s < 22.0$, $R - K_s > 3.35$; AB), all with deep *HST/ACS* imaging in B_{435} , V_{606} , i_{775} , and z_{850} , and well-calibrated photometric redshifts. Quantitative concentration and asymmetry measurements fail to separate EROs into distinct morphological classes. We therefore visually classify the morphologies of all EROs into four broad types: “Early” (elliptical-like), “Late” (disk galaxies), “Irregular” and “Other” (chain galaxies and low surface brightness galaxies), and calculate their relative fractions and comoving space densities. For a broad range of limiting magnitudes and color thresholds, the relative number of early-type EROs is approximately constant at 33–44%, and the comoving space densities of Early- and Late-type EROs are comparable. Mean rest-frame spectral energy distributions (SEDs) at $\lambda_{\text{rest}} \approx 0.1$ – $1.2\mu\text{m}$ are constructed for all EROs. The SEDs are extremely similar in their range of shapes, independent of morphological type. The implication is that any differences between the broad-band SEDs of Early-type EROs and the other types are relatively subtle, and there is no robust way of photometrically distinguishing between different morphological types with usual optical/near-infrared photometry.

Subject headings: surveys – galaxies: evolution – galaxies: fundamental parameters – galaxies: high-redshift – galaxies: stellar content – infrared: galaxies

1. INTRODUCTION

The newest challenges to galaxy formation models lie in predicting or explaining the state of galaxy assembly when the universe was in its middle ages, at only several billion years old. In field populations at these redshifts, $z \sim 1$ – 2 , it is necessary to sample a large enough volume at sufficient depth to overcome biases due to cosmic variance. This is particularly true for strongly clustered galaxies, such as the population of “extremely red objects” (EROs). These have comoving correlation scales of $\sim 10 h_{100}^{-1}$ Mpc at $z \gtrsim 1$ (Daddi et al. 2000a, 2002; Firth et al. 2002; Roche et al. 2002), and therefore require surveys of solid angle at least 100 arcmin² to have a variance less than $\sim 20\%$ (Somerville et al. 2003).

The spectral energy distributions (SEDs) of galaxies

¹ Based on observations taken with the NASA/ESA Hubble Space Telescope, which is operated by the Association of Universities for Research in Astronomy, Inc. (AURA) under NASA contract NAS 5-26555.

² Based on observations collected at the European Southern Observatory, Chile (ESO Programmes 164.O-0561, 168.A-0485, 169.A-0725, 170.A-0788, 267.A-5729)

³ Space Telescope Science Institute, 3700 San Martin Drive, Baltimore, MD 21218; leonidas, casertano, med, ferguson, mauro, koekemoer, somerville@stsci.edu

⁴ California Institute of Technology, Mail Stop 105-24, Pasadena, CA 91109; cc@astro.caltech.edu

⁵ Jet Propulsion Laboratory, California Institute of Technology, Mail Stop 169-327 (PE) & 169-506 (DS), Pasadena, CA 91109; prme@kromos.jpl.nasa.gov, stern@wolfkinder.jpl.nasa.gov

⁶ Department of Physics and Astronomy, The Johns Hopkins University, 3400 North Charles Street, Baltimore, MD 21218; nagrogin@stsci.edu

⁷ Steward Observatory, The University of Arizona, 933 North Cherry Avenue, Tucson, AZ 85721; papovich@as.arizona.edu

⁸ European Southern Observatory, Karl-Schwarzschild-Strasse 2, D-85748 Garching bei München, Germany; renzini@eso.org

are products of the amalgam of stellar mass functions, star formation histories, dust, and geometry, often with degeneracies (such as in age and metallicity) complicating interpretation. EROs, by their simple optical-minus-infrared color selection, embody this degeneracy extremely well, and are known to consist of at least two distinct classes of galaxies: old, and dusty/star-forming. Surveys in other wavelengths have post facto uncovered EROs, including radio (Willott et al. 2001), sub-mm (Smail et al. 2002; Wehner et al. 2002), and both hard- and soft-X-ray surveys (Alexander et al. 2002; Brusa et al. 2002). Each class (and subclass) of EROs offers a potentially important datum for further unfolding and challenging galaxy formation models. Currently, predictions of CDM-based semi-analytic models do not compare well against the numbers and statistics of EROs as a whole (Cimatti et al. 2002b; Firth et al. 2002). Having the relative fractions and space densities of, minimally, *morphologically*-determined early-type EROs versus all EROs (e.g. Yan & Thompson 2003), should improve the situation for comparisons against models.

Currently, there is a popular working hypothesis that some (large) fraction of EROs (those similar to the $z = 1.552$ 53W091, Spinrad et al. 1997) are the ancestors of present-day elliptical galaxies (e.g. Daddi et al. 2000b; Moustakas & Somerville 2002 [MS02]; and references therein). Conversely, many EROs demonstrably host highly obscured starbursts (e.g. the $z = 1.44$ HR10; Graham & Dey 1996) which could be an important component of the global luminosity density (Cimatti et al. 2002a; Elbaz et al. 2002). A photometric technique has been proposed by Pozzetti & Mannucci (2000) to make broad distinctions between passive and star-forming, dusty EROs. This is as yet not well-tested.

A systematic morphological and photometric study of a large, homogeneously-selected sample of EROs is therefore timely.

In this *Letter* we present the selection, morphological mix, and mean rest-frame SEDs of $K_s < 22.0$ (AB) EROs, selected from the GOODS-South *HST*/ACS mosaic (Giavalisco et al. 2003) over 163 arcmin². The sample selection and their redshifts are described in § 2, followed by the morphological study in § 3. In § 4 we present the relative fractions, space densities, and average rest-frame SEDs by morphological type. Conclusions are drawn in § 5. We give magnitudes in the AB system⁹, and, where necessary, we use a flat cosmology with $\Omega_m = 1 - \Omega_\Lambda = 0.3$ and $H_0 = 70 h_{70} \text{ km s}^{-1} \text{ Mpc}^{-1}$.

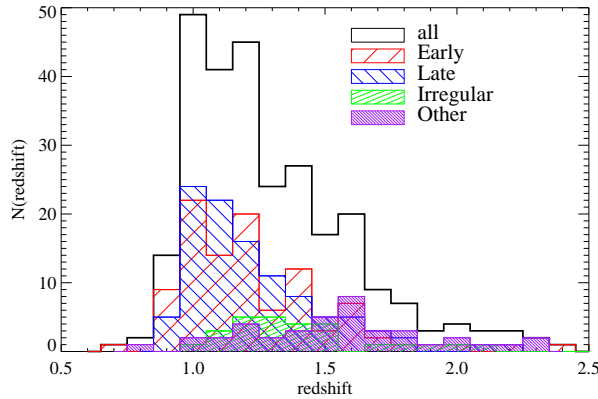


FIG. 1.— The ERO redshift distributions $N(z)$ for the full sample ($R - K_s > 3.35$, $K_s < 22.0$) and for each morphological type, as given in legend. The redshift distributions for Early- and Late-types are very similar, with $z_{\text{med}} \approx 1.2$, tailing to $z \sim 1.5$. The Irregular- and Other- types have a very broad $N(z)$ distribution with $z_{\text{med}} \approx 1.5$, and dominate the sample at $z \gtrsim 1.5$. Of the 275 objects plotted here, 66 redshifts are spectroscopic and the remainder are photometric (see text).

2. SAMPLE SELECTION AND REDSHIFTS

The GOODS data are described in Giavalisco et al. (2003). Briefly, for the Southern field (overlapping with CDFS; Giacconi et al. 2002), an ACS mosaic covering 163 arcmin² in B_{435} , V_{606} , i_{775} , and z_{850} are supported by a broad set of ground-based optical and infrared imaging, $U'UBVRIJHK_s$, from the VLT, NTT, and 2.2 m telescopes. The infrared data are from the SOFI and ISAAC instruments. For this work, we employ a PSF-matched SOFI K_s -selected catalog from which the stars have been removed¹⁰. The SOFI data reach $\sim 50\%$ completeness at $K_s \approx 22.8$, and are still nearly entirely complete at $K_s \approx 22.0$ (Giavalisco et al. 2003; Moy et al. 2003).

We consider several definitions of EROs, all of which are essentially complete for these survey depths: three color cuts ($R - K_s > 3.35$, 3.65, and 4.35) for each of two magnitude limits ($K_s < 21.0$ and 22.0). The largest (“full”) sample ($R - K_s > 3.35$, $K_s < 22.0$) consists of 275 objects. The smallest sample ($R - K_s > 4.35$, $K_s < 21.0$) contains 18 objects.

⁹ The most relevant conversions to Vega magnitudes and colors for this paper are: $R_{\text{Vega}} = R - 0.206$ and $K_s, \text{Vega} = K_s - 1.859$. Thus, $R - K_s > 3.35$ in AB corresponds to $(R - K_s)_{\text{Vega}} > 5.0$.

¹⁰ Unresolved sources are identified by a plot of the z_{850} 0.0625 arcsec-diameter surface-brightness vs isophotal magnitude, which provides a robust separation to $z_{850} \approx 26.5$.

Photometric redshifts are computed using the method of Benítez (2000). These are well-calibrated to $z_{\text{spec}} \approx 1.5$, with $\sigma[\Delta z/(1 + z_{\text{spec}})] = 0.11$ (to $R < 25.5$; Mobasher et al. 2003) using a total of 434 spectroscopic redshifts, including 202 from a VLT/FORS2 campaign over 2002-2003 (to be presented elsewhere), and from the K20 survey (Cimatti et al. 2002b,c). This sample includes 66 EROs with $R - K_s > 3.35$ and $K_s < 22.0$, for which $\sigma[\Delta z/(1 + z_{\text{spec}})] = 0.05$. In the analysis that follows, photometric redshifts have been replaced with spectroscopic redshifts where possible. There is one faint compact ERO with a formal $z_{\text{phot}} = 6.4$, which is a candidate L -dwarf; for completeness we keep this object in the full sample. The ERO redshift distribution for the full sample is shown in Fig. 1. The $N(z)$ has a fairly sharp edge at $z \approx 0.95$, a median value of $z_{\text{med}} \approx 1.2$. The $N(z)$ for the redder subsets are similar, but shifted to a higher median redshift, $z_{\text{med}} \approx 1.5$ (for $R - K_s > 4.35$).

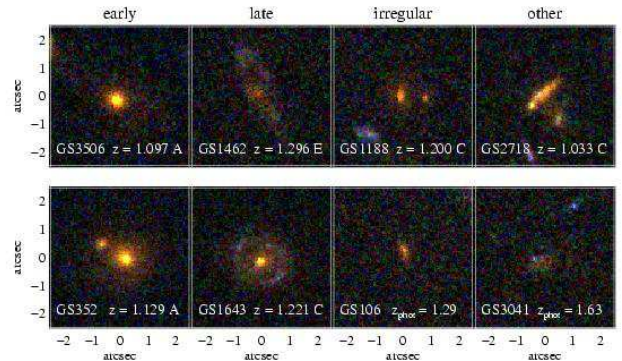


FIG. 2.— Montage of 3-color Biz stamps, illustrating examples of each morphological type, as described in the text. Two objects are given for each type (by column). The caption of each stamp gives the ID (“GS”=GOODS-South); the redshift (spectroscopic for all but for GS 106 and GS 3041, for which photometric redshifts are given); and a letter code reflecting observed spectroscopic features – A=absorption; E=emission; C=both emission and absorption features.

3. MORPHOLOGICAL CLASSIFICATION OF EROS

The study of EROs has been largely motivated by their tantalizing connection with both the progenitors of present-day massive elliptical galaxies, and possibly, ultraluminous infrared galaxies. Using the high-resolution ACS data, it should be possible to distinguish between these extremes morphologically. With the ACS z_{850} data, restframe morphologies longward of 4000Å can be determined for redshifts $z \lesssim 1.3$, reducing possible morphological k -correction issues (e.g. Giavalisco et al. 1996) for most EROs in this sample. The GOODS data reach a z_{850} 1- σ isophotal limit of 27.3 mag arcsec⁻² (Giavalisco et al. 2003). As the average magnitude of galaxies in the full sample is $z_{850} \approx 23.0$, for most cases the distinction between early- and non-early-types should be clear. At redshifts beyond $z \approx 1.3$, the 4000Å-break begins to shift past the z_{850} band, and morphological k -corrections may become important. This can be solved by also examining longer-wavelength imaging (e.g. the ~ 0.4 arcsec-resolution ISAAC data in the K_s -band); this will be done in future work.

We began by exploring the galaxy morphologies with the concentration and asymmetry (CAS) param-

eters of Conselice (2003, see also Abraham et al. 1996; Bershady et al. 2000). We found that the parameter values were fairly continuous and did not cleanly distinguish “classes,” which reflects the morphological richness of all types of EROs. We therefore resorted to a *visual* classification approach, and report the range and spread of the resulting by-type CAS values below.

We adopt four broad morphological types: Early, Late, Irregular, and Other. The classification is based largely on the z_{850} data, with cross-examination of the B_{435} , V_{606} , and i_{775} imaging for the colors and multi-wavelength structure of features. Since a primary goal of this work is to make a census of EROs that may be present-day elliptical progenitors, we use a conservative definition for Early types, excluding galaxies with any definite evidence of a prominent disk or dust-band. An isolated environment was not a requirement, so included are galaxies that are clearly interacting or merging. The Late-type category consists of galaxies with some regular, disk-like component, independent of the bulge fraction – which can be quite large. Irregular-types are the Magellanic-type galaxies, whereas the Other type predominantly includes low surface brightness galaxies and chain galaxies with multiple star-formation sites. Two examples of each type are given in Fig. 2.

The classifications were done independently by four authors (SC, PE, RL, LAM), with the consolidation done by LAM. The overall agreement was very good, the greatest differences arising in the use of galaxies’ central concentration as a criterion for several cases of morphologically Early-type galaxies. Since it became apparent that many EROs appear to be in dynamical disequilibrium, potentially softening the sharpness of cores, concentration as a criterion was relaxed.

For both Early- and Late-type EROs, the mean values and typical dispersions of the CAS parameters, are $C_E \approx C_L \approx 3.1 \pm 0.5$, and $A_E \approx A_L \approx 0.25 \pm 0.1$. The Irregular- and Other-type EROs are both less concentrated (at $C_I \approx C_O \approx 2.5 \pm 0.3$) and more asymmetric (at $A_I \approx A_O \approx 0.3 \pm 0.2$).

4. RESULTS

The full ERO dataset comprises $\sim 10\%$ of all K_s -selected galaxies at $K_s = 20\text{--}22$. The relative fractions of EROs by morphological type are presented in Table 1 for several limiting magnitudes and color limits. We find the relative fraction of Early-types does not depend strongly on the selection criteria, staying at 33 – 44% of the total numbers. Late-types, however, dominate the population at brighter magnitudes (with 55% at $K_s < 21.0$, $R - K_s > 3.35$), and comprise much smaller fractions (23%) at the faintest, reddest limit (see also I_{F814W} -band WFPC2-based analyses by Yan & Thompson 2003 and Gilbank et al. 2003, which find similar relative fractions). The redshift distributions of Early- and Late-types are very similar (Fig. 1). The combined fraction of Irregular- and Other-types increases dramatically with both limiting magnitude and color threshold; these galaxies also tend to have higher photometric redshifts, with a median of $z_{\text{med}} \approx 1.5$. Based on the observed redshift distributions, comoving space densities are calculated and presented in Table 2. The volume probed by the full sample is $\sim 4.4 \times 10^5 h_{70}^{-3} \text{Mpc}^3$, for a total comoving space density of $n = (6.40 \pm 0.39) \times 10^{-4} h_{70}^3 \text{Mpc}^{-3}$, and

the cosmic variance uncertainty is therefore $\sigma_{\text{cv}} \approx 15\%$ (Somerville et al. 2003).

To explore whether there is a useful correspondence between morphological type and colors, we calculate the rest-frame SED of each ERO, normalized to $f_\nu = 1$ (arbitrary units) at 5200 Å. In Fig. 3 we plot all data points for two groupings of morphological types, with the corresponding mean “blue” and “red” SEDs, as described in the caption. The strong break around 4000 Å follows from the red-color selection of EROs. It is interesting that the range of SED shapes is extremely similar for all EROs. This is reflected also in the formal SED-fitting done for calculating photometric redshifts in Mobasher et al. (2003). Even the reddest normal starburst SEDs (drawn from Kinney et al. 1996) are too blue to fit EROs, so the EROs tend strongly to be best-fit by the earliest (elliptical) SED templates. As seen in the inset of Fig. 3, the empirical SED of the ultraluminous infrared galaxy (ULIRG) Arp 220 (as given in Elbaz et al. 2002) is sufficiently red to match ERO colors, and is coincidentally remarkably similar to the SED of an old, passively-evolved, unreddened system. Many of the Late-type galaxies have large bulges, and so their SEDs may naturally be dominated by old stellar populations. Even the Irregular and Other morphological types alone, which may arguably be candidates for ULIRGs, span the same range of SED shapes shown in Fig. 3. We conclude that in this wavelength-range, color information is insufficient to *generally* distinguish between clearly distinct morphological types of EROs.

5. CONCLUSIONS

Samples of color-selected EROs consist of several distinct galaxy types for all magnitude ranges and color-cuts. All morphological types are found over very similar redshift ranges, $z_{\text{med}} \approx 1.2$, with the more morphologically-disturbed (Irregular and Other) types tending to somewhat higher redshifts. This may be due to a combination of a morphological k -correction selection effects (where at redshifts above $z \approx 1.3$ galaxy bulges may be less apparent in the z_{850} data); and a hint of a population of real, “train-wreck” galaxies, seen at redshifts closer to $z \approx 2$. With the present data, it is not possible to distinguish between these possibilities from the photometry alone, as seen by the grossly-similar rest-frame SEDs of all morphological types. This does suggest that those EROs that *are* perhaps “dusty starbursts,” have SEDs that are more similar to local ULIRGs (such as Arp 220), rather than (mere) starburst galaxies.

The comoving space density of morphologically Early-type EROs ($n_E \approx 2.5 \times 10^{-4} h_{70}^3 \text{Mpc}^{-3}$) is quite comparable to present-day giant Ellipticals, $n_{\text{gE}, z=0} \approx 2.1 \times 10^{-4} h_{70}^3 \text{Mpc}^{-3}$ (c.f. MS02). This suggests that the $z \approx 1.2$ Early-type galaxies identified within the ERO population may in fact correspond to the majority of the most massive ellipticals today, pointing to an epoch of assembly, as well as star-formation, at redshifts well beyond $z > 2$.

We acknowledge discussion at many stages of this work with D. Alexander and F. Bauer, and comments by L. Yan. The work of DS was carried out at JPL, Caltech,

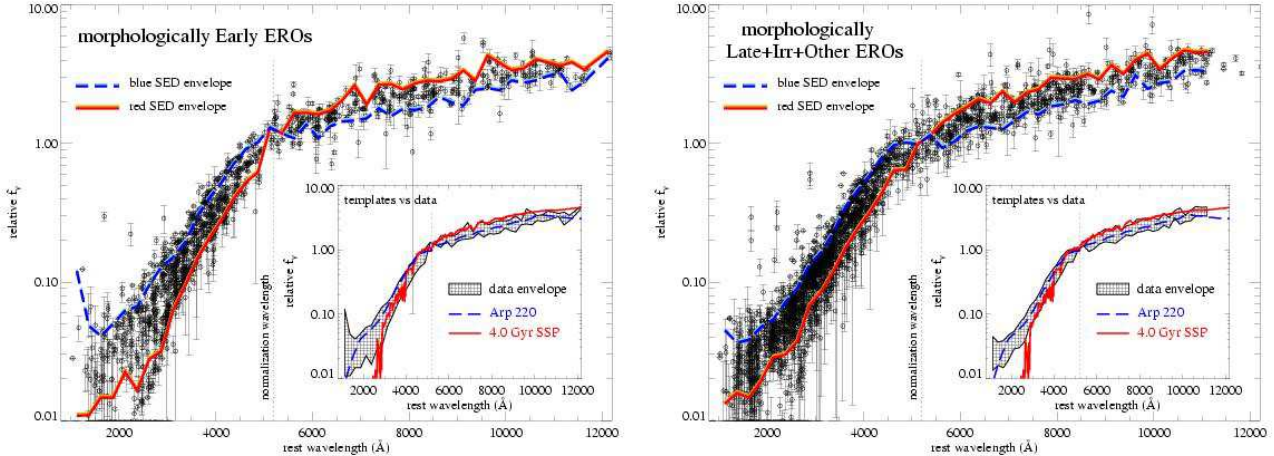


FIG. 3.— The rest-frame SEDs for $K_s < 22$, $R - K_s > 3.35$ EROs, Early at left; the combined set of Late, Irregular, and Other types combined, at right. These are constructed from the broadband magnitudes, shifted to the restframe via photometric and spectroscopic redshifts. All SEDs are normalized to $f_v = 1$ at 5200 Å, with the precise normalization value for each object determined via interpolation on the best-fitting SED from Mobasher et al. (2003). All points are shown with their photometric uncertainty – some of the error bars are smaller than the points. At each wavelength bin, a bi-weight mean and dispersion are calculated; these can then be compared against two representative ERO templates, shown in the inset plot: the Arp 220 SED (as given in Elbaz et al. 2002); and a 4.0 Gyr old $Z = Z_\odot$ simple stellar population from the v.2000 Bruzual & Charlot (1993) models.

under a contract with NASA. Support for this work, part of the *Space Infrared Telescope Facility (SIRTF)* Legacy Science Program, was provided by NASA through con-

tract number 1224666 issued by the Jet Propulsion Laboratory, California Institute of Technology under NASA contract 1407.

REFERENCES

Abraham, R. G., Tanvir, N. R., Santiago, B. X., Ellis, R. S., Glazebrook, K., & van den Bergh, S. 1996, MNRAS, 279, L47
 Alexander, D. M., Vignali, C., Bauer, F. E., Brandt, W. N., Hornschemeier, A. E., Garmire, G. P., & Schneider, D. P. 2002, AJ, 123, 1149
 Benítez, N. 2000, ApJ, 536, 571
 Bershadsky, M. A., Jangren, A., & Conselice, C. J. 2000, AJ, 119, 2645
 Bolzonella, M., Miralles, J.-M., & Pelló, R. 2000, A&A, 363, 476
 Brusa, M., Comastri, A., Daddi, E., Cimatti, A., Mignoli, M., & Pozzetti, L. 2002, ApJL, 581, L89
 Bruzual, A. G., & Charlot, S. 1993, ApJ, 405, 538
 Cimatti, A., et al. 2002a, A&A, 381, L68
 Cimatti, A., et al. 2002b, A&A, 391, L1
 Cimatti, A., et al. 2002c, A&A, 392, 395
 Conselice, C. J. 2003, ApJS, 147, 1
 Daddi, E., et al. 2000a, A&A, 361, 535
 Daddi, E., Cimatti, A., Renzini, A. 2000b, A&A, 362, L45
 Daddi, E., et al. 2002, A&A, 384, L1
 Elbaz, D., Flores, H., Chanial, P., Mirabel, I. F., Sanders, D., Duc, P.-A., Cesarsky, C. J., & Aussel, H. 2002, A&A, 381, L1
 Firth, A. E., et al. 2002, MNRAS, 332, 617
 Giacconi, R., et al. 2002, ApJS, 139, 369
 Giavalisco, M., Livio, M., Bohlin, R. C., Macchetto, F. D., & Stecher, T. P. 1996, AJ, 112, 369
 Giavalisco, M. et al. 2003, ApJL, in press
 Gilbank, D. G., Smail, I., Ivison, R. J., & Packham, C. 2003, preprint (astro-ph/0308318)
 Graham, J. R. & Dey, A. 1996, ApJ, 471, 720
 Kinney, A. L., Calzetti, D., Bohlin, R. C., McQuade, K., Storchi-Bergmann, T., & Schmitt, H. R. 1996, ApJ, 467, 38
 Mobasher, B. et al. 2003, ApJL, in press
 Moriondo, G., Cimatti, A., & Daddi, E. 2000, A&A, 364, 26
 Moustakas, L. A., Davis, M., Graham, J. R., Silk, J., Peterson, B. A., & Yoshi, Y. 1997, ApJ, 475, 445
 Moustakas, L. A. & Somerville, R. S. 2002, ApJ, 577, 1 (MS02)
 Moy, E., Barmby, P., Rigopoulou, D., Huang, J.-S., Willner, S. P., & Fazio, G. G. 2003, A&A, 403, 493
 Pozzetti, L. & Mannucci, F. 2000, MNRAS, 317, L17
 Roche, N. D., Almaini, O., Dunlop, J., Ivison, R. J., & Willott, C. J. 2002, MNRAS, 337, 1282
 Smail, I., Owen, F. N., Morrison, G. E., Keel, W. C., Ivison, R. J., & Ledlow, M. J. 2002, ApJ, 581, 844
 Somerville, R. S. et al. 2003, ApJL, in press
 Spinrad, H., Dey, A., Stern, D., Dunlop, J., Peacock, J., Jimenez, R., & Windhorst, R. 1997, ApJ, 484, 581
 Wehner, E. H., Barger, A. J., & Kneib, J. P. 2002, ApJ, 577, L83
 Willott, C. J., Rawlings, S., & Blundell, K. M. 2001, MNRAS, 324, 1
 Yan, L. & Thompson, D. 2003, ApJ, 586, 765

TABLE 1
ERO FRACTIONS (%) BY MORPHOLOGICAL TYPE*

	$R - K_s >$	$K_s < 21.0$			$K_s < 22.0$		
		3.35	3.65	4.35	3.35	3.65	4.35
<i>early</i>		36	41	44	37	38	33
<i>late</i>		55	52	39	38	32	23
<i>irregular</i>		5.1	5.5	17	11	12	23
<i>other</i>		2.5	1.4	0.0	15	17	20
total number[†]		118	73	18	275	185	60

*: The relative fractions are given in percent (%).

†: Total number of EROs with shown criteria.

TABLE 2
ERO SPACE DENSITIES [$\times 10^{-4} h_{70}^3 \text{ Mpc}^{-3}$] BY MORPHOLOGICAL TYPE*

	$K_s < 21.0$			$K_s < 22.0$		
	$R - K_s > 3.35$	$R - K_s > 3.65$	$R - K_s > 4.35$	$R - K_s > 3.35$	$R - K_s > 3.65$	$R - K_s > 4.35$
<i>early</i>	1.10 ± 0.17	0.67 ± 0.12	0.09 ± 0.03	2.49 ± 0.25	1.59 ± 0.19	0.29 ± 0.07
<i>late</i>	1.45 ± 0.18	0.86 ± 0.14	0.14 ± 0.05	2.36 ± 0.23	1.37 ± 0.18	0.25 ± 0.07
<i>l+i+o[†]</i>	1.67 ± 0.19	0.98 ± 0.15	0.17 ± 0.05	3.84 ± 0.29	2.53 ± 0.24	0.72 ± 0.11
<i>all</i>	2.94 ± 0.27	1.64 ± 0.19	0.26 ± 0.06	6.40 ± 0.39	4.11 ± 0.30	1.03 ± 0.13

*: The space density of EROs with specified $R - K_s$ and K_s thresholds, in units of $10^{-4} h_{70}^3 \text{ Mpc}^{-3}$, with Poisson uncertainties.

†: Results for the combined numbers of Late-, Irregular-, and Other-type EROs.